Room-Temperature All-Solid-State Lithium–Organic Batteries Based on Sulfide Electrolytes and Organodisulfide Cathodes

Zihao Yang, Feng Wang, Zijun Hu, Jun Chu, Hui Zhan, Xinping Ai,* and Zhiping Song*

All-solid-state design is effective to address the challenges of Lithium–organic batteries, such as the dissolution of organic electrode materials (OEMs) and the safety of the Li anode. However, previous attempts, based on carbonyl-type OEMs failed to achieve acceptable electrochemical performance in room-temperature all-solid-state Li batteries (ASSLBs). Herein, the authors report the first organodisulfide cathode, poly(trithiocyanuric acid) (PTTCA), for ASSLBs. By compositing with carbon nanotubes to enhance the electronic conductivity and using the sulfide electrolyte, $Li_7P_3S_{11}$, to build an electrochemically favorable interface, PTTCA demonstrates an electrochemical performance superior to all the OEMs reported so far in ASSLBs at room temperature, including a reversible capacity of 410 mAh g^{-1}, an energy density of 767 Wh kg^{-1}, and a capacity retention of 83% after 100 cycles. It is believed that this work provides new orientation and insights for the further development of both ASSLBs and OEMs.

1. Introduction

Organic electrode materials (OEMs) have received increasing attentions in recent years due to their promising electrochemical performance and other unique advantages including structural diversity, property designability, and resource sustainability.[1] However, the practical applications of OEMs, especially the intensively investigated n-type ones, face two major challenges: first, most small molecules and low-molecular-weight polymers (including their discharged forms) dissolve in liquid electrolytes and result in poor cycling stability; second, as the primary application of n-type OEMs, lithium (Li)–organic batteries rely on a thorough settlement of the rechargeability and safety issues of Li metal anode. Many efforts (such as immobilization,[2] polymerization,[3] and electrolyte optimization[4]) have been made to alleviate or solve the dissolution problem, however, at the expense of significantly reduced energy density

or/and elevated cost. Besides, the problems of Li metal anode have not been seriously considered for Li–organic batteries at current stage, which may learn from the experience of other Li-metal-based systems such as Li–inorganic, Li–S, and Li–air batteries.

All-solid-state Li batteries (ASSLBs) are regarded as the final solution of Li-metal-based batteries because of the intrinsic safety. In our opinion, even apart from this advantage, the application of OEMs in ASSLBs is probably a win–win strategy. On one hand, solid electrolytes with inherent immobility can absolutely prevent the dissolution and shuttle of OEMs. On the other hand, OEMs have many unique properties suitable for ASSLBs compared to other kinds of cathode materials: higher flexibility and processability than rigid inorganics for intimate contact with solid electrolyte, lower requirements on the electrochemical window of solid electrolyte (generally below 4.0 or 3.5 V vs Li$^+$/Li) than inorganics, faster redox kinetics, and smaller volume variation than S and air cathodes.[5] However, in spite of so many merits, successful examples of organic cathode materials for ASSLBs are still very lacking, especially those can work at room temperature. Among all kinds of solid electrolytes, sulfide electrolyte is the most appropriate choice to construct room-temperature ASSLBs because of the highest ionic conductivity ($>10^{-3}$ S cm^{-1}) and good processability.[6] In very recent years, a few OEMs including carbonyl-type COF-TRO[7] and PTO,[8] and azo-type PBALS[9] have been tried as cathode for ASSLBs based on sulfide electrolytes. Unfortunately, carbonyl-type ones cannot release their capacity until at a high temperature like 60 °C,[7,8] while PBALS can only deliver a low reversible capacity of 128 mAh g^{-1} at room temperature.[9] For carbonyl-type cathode materials that attract most attentions in the field of OEMs, their poor performance at room temperature can be well explained by the hard and soft acids and bases (HSAB) theory.[10] As a hard base, O of H_2O preferentially reacts with the hard acid P of sulfide electrolyte to replace the soft base S,[11] which has been evidenced by the easy deliquescence of sulfide electrolytes in air. Similarly, the hard base O of discharged carbonyl group (C—O$^-$) should also interact with the hard acid P of sulfide electrolyte, hindering the redox reaction of carbonyl group. Therefore, it is necessary to elevate the temperature to weaken their interaction for improving the utilization of active

Z. Yang, F. Wang, Z. Hu, J. Chu, H. Zhan, X. Ai, Z. Song
Hubei Key Lab of Electrochemical Power Sources
College of Chemistry and Molecular Sciences
Wuhan University
Wuhan 430072, China
E-mail: xpai@whu.edu.cn; zpsong@whu.edu.cn

**ADVANCED
SCIENCE NEWS**
www.advancedsciencenews.com

**ADVANCED
ENERGY
MATERIALS**
www.advenergymat.de

material. Similar results have been also found in all-solid-state sodium batteries (ASSSBs) based on sulfide electrolytes and carbonyl cathodes.[12]

Based on the above understanding, for achieving high utilization and high capacity at room temperature, a possible solution is to use OEMs with softer electroactive groups, for example, S—S bond. In fact, organodisulfides have many merits including high theoretical capacity and low cost, and thereby have been intensively studied in the 1990s and 2000s.[13] However, suffering from the serious dissolution, the research progress on organodisulfide electrode materials is very limited in the last decade. Nowadays, the rise of ASSLBs probably provides organodisulfides new opportunities to solve the dissolution problem and thus give full play to their electrochemical performance. Herein, we report poly(trithiocyanuric acid) (PTTCA) as the first organodisulfide cathode material for ASSLBs. PTTCA is an easily synthesized polymer from low-cost trithiocyanuric acid (TTCA), and own an attractive theoretical capacity of 450 mAh g^{-1}. In conventional liquid electrolytes, PTTCA itself is insoluble, but its discharge products are soluble. With the gradual breakage of S—S bonds during discharge, the dissolution becomes more and more serious, resulting in poor cycling performance.[14] In this work, we choose a commercial sulfide

electrolyte, Li$_7$P$_3$S$_{11}$ (LPS), to realize a room-temperature all-solid-state Li–PTTCA battery. Besides the synthesis, characterizations, and electrochemical performance of PTTCA, the effect of conductive carbon (Super P [SP] and carbon nanotubes [CNTs]) in the PTTCA@C composite, interaction between LPS and PTTCA, and comparison between organodisulfide (PTTCA) and carbonyl cathodes (poly(anthraquinonyl sulfide) [PAQS]) in ASSLBs, have also been carefully investigated. We believe, this work not only reports an electrochemical performance breakthrough, but also provides new orientation and insights for the further development of all-solid-state Li–organic batteries.

2. Results and Discussion

2.1. Preparations and Characterizations of Cathode Materials

PTTCA was synthesized by a simple one-pot oxidation polymerization using Li$_3$TTCA (the trilithium salt of TTCA) as monomer and I$_2$ as oxidizer[14a,15] (**Figure 1**a). For efficient utilization of conductive carbon in the cathode, PTTCA@SP and PTTCA@CNT composites were also prepared by an in situ polymerization method with similar procedures.
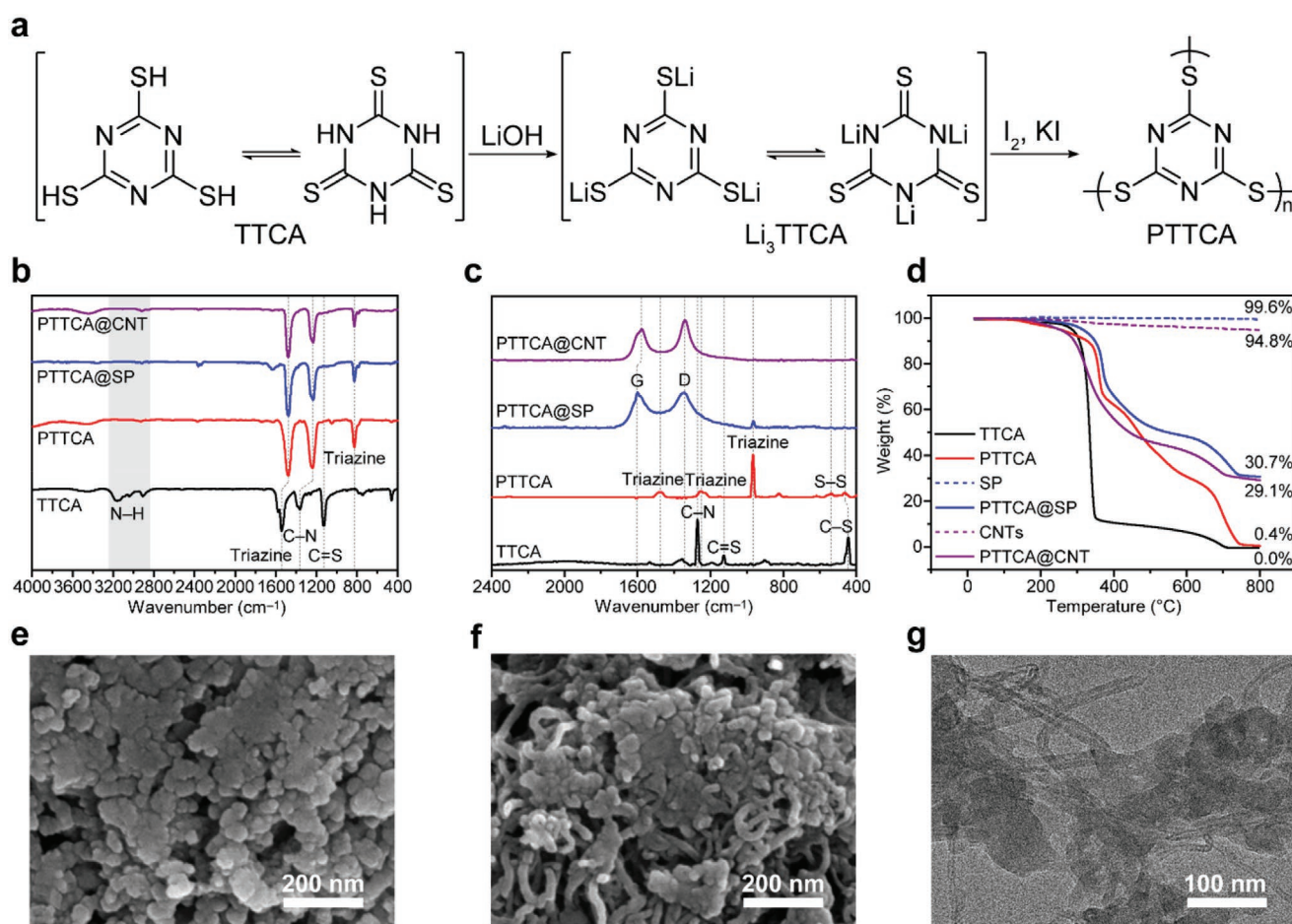
Figure 1. a) Synthetic route to PTTCA, with the resonant structure of TTCA and Li$_3$TTCA. b) FT-IR and c) Raman spectra of the four samples including TTCA, PTTCA, PTTCA@SP, and PTTCA@CNT. d) TG curves of the four samples as well as SP and CNTs for calculation (nitrogen atmosphere, 25–800 °C, 10 °C min^{-1}). SEM images of e) PTTCA@SP and f) PTTCA@CNT composites. g) TEM image of PTTCA@CNT composite.

2102962 (2 of 10)

ADVANCED
SCIENCE NEWS
www.advancedsciencenews.com

ADVANCED
ENERGY
MATERIALS
www.advenergymat.de

Fourier transform infrared (FT-IR, Figure 1b) and Raman spectra (Figure 1b) were used to confirm the successful synthesis of PTTCA (detailed peak assignments are listed in Tables S1 and S2, Supporting Information, respectively). In the FT-IR spectra, the peaks of N−H (3150–2900 cm^{-1}) and C=S (1125 cm^{-1}) bonds ascribed to the resonance thione structure of TTCA,[16] completely disappeared for PTTCA and its composites. Additionally, the peaks at 1540 and 1360 cm^{-1} (for the stretching vibrations of triazine ring and C−N bond, respectively) red-shifted and a new peak at 825 cm^{-1} (for the out-of-plane bending vibration of symmetrical triazine ring[17]) appeared for PTTCA and its composites. These obvious variations and the high consistency of the spectra of PTTCA, PTTCA@SP, and PTTCA@CNT indicated the successful polymerization of the three samples. In the Raman spectra, the peaks at 1225 and 1125 cm^{-1} (for the stretching vibrations of C−N and C=S bonds,[17] respectively) disappeared while the peaks at 968 and 540 cm^{-1} (for the bending vibration of in-phase N-radial ring and the stretching vibration of S−S bond,[18] respectively) appeared after polymerization. As for PTTCA@SP and PTTCA@CNT, the characteristic G and D bands of graphitic carbon confirmed the existence of SP or CNTs in the composite. Due to the optical absorption of carbon and high intensities of G and D bands, the characteristic peaks of PTTCA were difficult to be identified. Especially for PTTCA@CNT, the higher surface area or more homogeneous distribution of CNTs compared to SP made the Raman signals of PTTCA completely hidden.

There were also huge differences between the X-ray diffraction (XRD) patterns (Figure S1, Supporting Information) of TTCA and PTTCA. In contrast to the crystalline feature of TTCA, PTTCA and its composites showed only a weak and broad peak, indicating the amorphous feature of the polymer. To evaluate the PTTCA contents in PTTCA@SP and PTTCA@CNT, both thermogravimetric (TG, Figure 1d) analysis and elemental analysis (EA, Table S3, Supporting Information) were conducted for these samples. After heating to 800 °C in N$_2$ atmosphere, PTTCA@SP and PTTCA@CNT retained 30.7% and 29.1% of the initial weight, respectively, while PTTCA almost completely decomposed (with only 0.4% weight left) but SP and CNTs were highly thermostable (with 99.6% and 94.8% weight retentions, respectively). According to Equation S1, Supporting Information, the content of PTTCA was calculated to be 69.5% in PTTCA@SP or 69.6% in PTTCA@CNT, respectively. The inductively coupled plasma mass spectroscopy (ICP–MS, Table S3, Supporting Information) suggested that residual metal elements (Li and K) were negligible in PTTCA. Since PTTCA was the only source of N and S in the composites, its content could be also deduced by the relative proportion of the two elements (Equations S2 and S3, Supporting Information). The results were 68.6% or 69.3% in PTTCA@SP, and 69.3% or 66.3% in PTTCA@CNT, respectively, which agreed well with the TG analysis. Summarizing these data and taking possible errors into account, we could draw a conclusion that PTTCA occupied ≈70% of the weight of either PTTCA@SP or PTTCA@CNT sample.

Scanning electron microscopy (SEM) images were recorded to reveal the morphology of PTTCA@SP and PTTCA@CNT composites. For PTTCA@SP, it was difficult to distinguish SP from PTTCA because their particles were quite similar (with
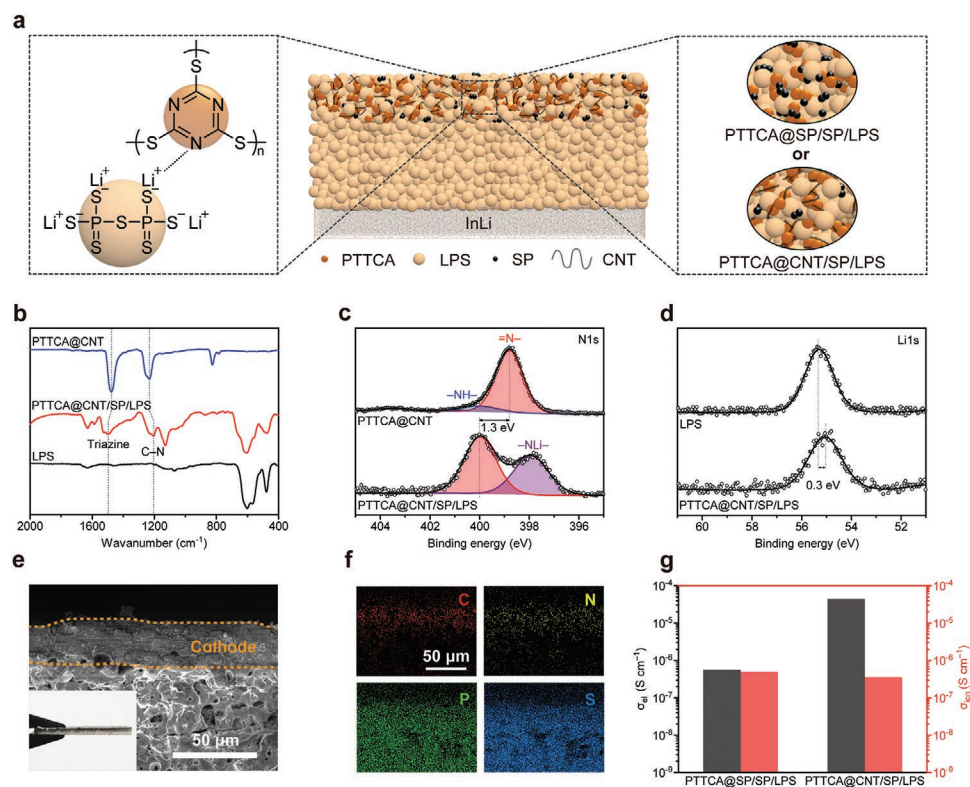
small dimensions of about 50 nm) and homogeneously distributed to form aggregations (Figure 1e and Figure S2c, Supporting Information). As for PTTCA@CNT, uniform distribution of CNTs and PTTCA was also observed without obvious bundling of CNTs (Figure 1g and Figure S2d, Supporting Information). Transmission electron microscopy (TEM) observation further clarified that small PTTCA particles with small dimensions of about 50 nm aggregated on the surfaces of CNTs with diameters of about 20 nm (Figure 1g). All the above results verified the highly homogeneous mixing of PTTCA with SP or CNTs in the composites, which was expected to facilitate the electron transport in the cathode with limited proportion of conductive carbon.

2.2. Characterizations and Properties of Cathode Composites

The as-prepared PTTCA@SP or PTTCA@CNT sample was ball-milled with LPS and additional SP to form the cathode composite (named as PTTCA@SP/SP/LPS or PTTCA@CNT/SP/LPS, respectively) for ASSLBs, with an appropriate weight ratio of PTTCA/(CNT + SP)/LPS = 30:15:55. To assemble an all-solid-state cell, the cathode composite was pressed onto one side of the LPS electrolyte pellet, while the InLi alloy anode was tightly attached on the other side (**Figure 2**a, middle). InLi was used to replace Li anode because it has much better compatibility with sulfide electrolyte due to higher and constant redox potential (0.6 V vs Li$^+$/Li).[19] It has been accepted as a common practice for sulfide-electrolyte-based ASSLBs, as to focus research attention on the compatibility between electrolyte and cathode active material.

Besides physical contact, there might exist some chemical interactions between LPS and PTTCA according to their structure features. To evidence this speculation, we took PTTCA@CNT/SP/LPS cathode composite as an example to characterize the FT-IR spectra (Figure 2b) and X-ray photoelectron spectra (XPS, Figure 2c,d and Figure S3, Supporting Information). After ball milling, the FT-IR peak corresponding to the stretching vibration of C−N bond, red-shifted from 1235 cm^{-1} for PTTCA@CNT to 1205 cm^{-1} for PTTCA@CNT/SP/LPS, suggesting that the vibration was stabilized by the formation of Li$^+$···N coordination bond[20] between LPS and PTTCA (Figure 2a, left). In addition, the peak corresponding to the stretching vibration of aromatic trithiol form of triazine ring, blue-shifted from 1478 to 1495 cm^{-1}, indicating a lowered conjugacy of the aromatic ring due to the formation of Li$^+$···N bond. Significant differences were also observed in the XPS data, especially N1s (Figure 2c) and Li1s spectra (Figure 2d). The N element in PTTCA@CNT was dominantly in =N− form (398.8 eV), with minor existence of −NH− form (400.1 eV) ascribed to the terminal groups of PTTCA with residual H atoms (Table S3, Supporting Information).[20] After ball milling with LPS and SP, the =N− peak split into two peaks located at 397.9 and 400.1 eV, respectively. The lower one (397.9 eV) could be assigned to −NLi− (or >N$^-$···Li$^+$) form, where the electron density on N atoms increased due to partial reduction of PTTCA by LPS.[21] In the S2p spectrum (Figure S3a, Supporting Information), the relative intensities of C=S and P−S−P increased after ball milling, which might be the clues of the

**ADVANCED
SCIENCE NEWS**

www.advancedsciencenews.com
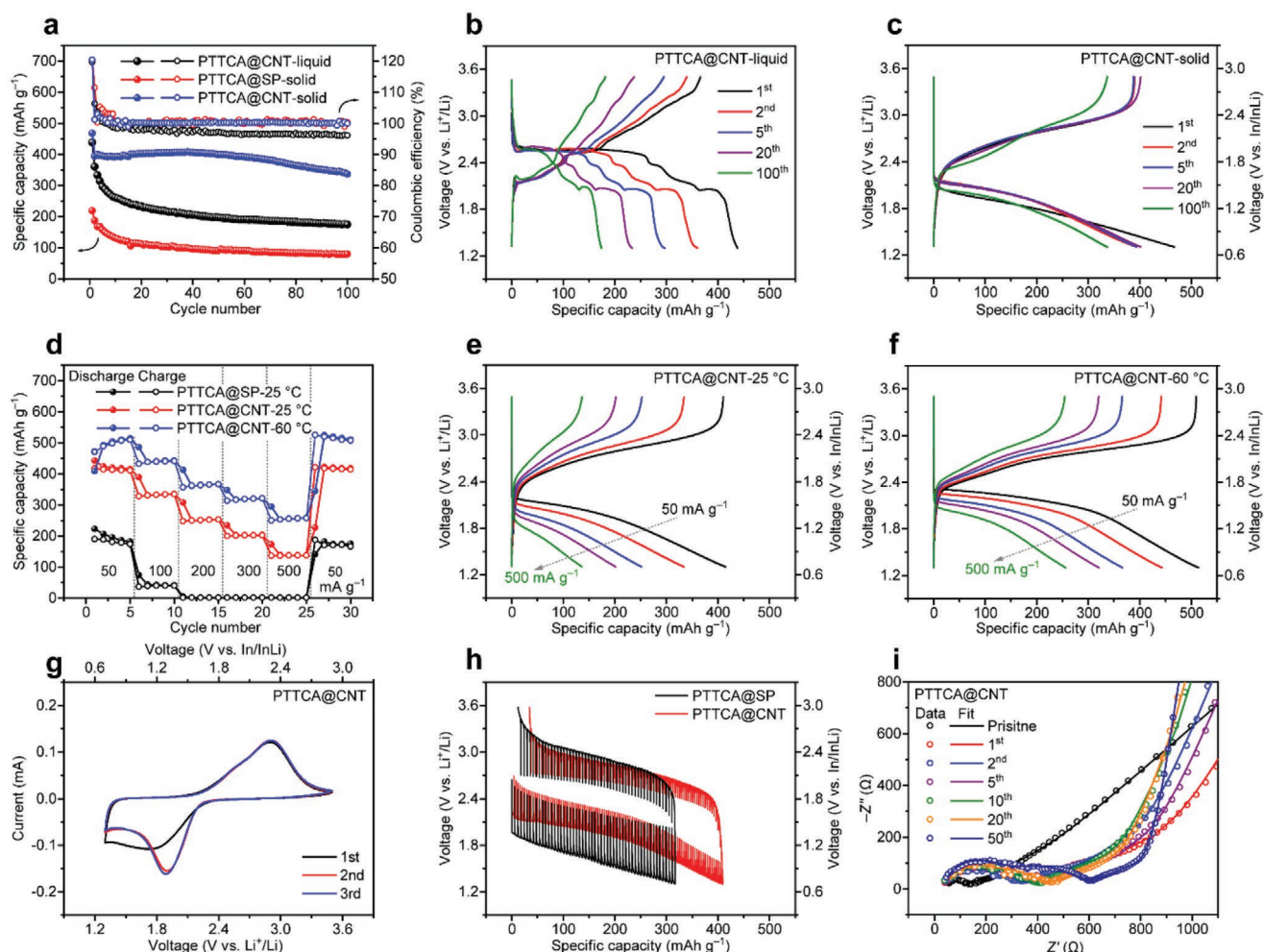
**ADVANCED
ENERGY
MATERIALS**

www.advenergymat.de

Figure 2. a) Schematic illustrations of the ASSLB based on LPS electrolyte and PTTCA cathode (middle), interaction between LPS and PTTCA in the cathode (left), and detailed architectures of cathodes using PTTCA@SP and PTTCA@CNT composites (right). b) FT-IR spectra of PTTCA@CNT/SP/LPS cathode composite, as well as LPS and PTTCA@CNT for comparison. c,d) XPS spectra of PTTCA@CNT/SP/LPS cathode composite, as well as LPS and PTTCA@CNT for comparison. e,f) SEM and EDS mapping images of the cross section of the pellet containing electrolyte and cathode layers, with digital photograph of the pellet shown as an insertion in (e). g) Column chart of electronic and ionic conductivities of PTTCA@SP/SP/LPS and PTTCA@CNT/SP/LPS cathode pellets.

formation of Li_3TTCA[20] and $P_2S_7^{4-}$[8b,22] as the reduction product of PTTCA and the oxidation product of LPS, respectively. The binding energy of $=N-$ group shifted toward higher value ($\Delta E_b = 400.1$ eV $- 398.8$ eV $= 1.3$ eV), again verified the $Li^+\cdots N$ coordination because Li^+ lowered the electron density on N atoms.[23] The Li1s spectrum showed a shift of 0.3 eV toward lower binding energy, further confirming the formation of ionic bond or coordination bond between Li^+ and negatively charged or neutral N atom, respectively.[24] As a summary, the significant variations in FT-IR and XPS data revealed that the redox reaction and coordination interaction extensively occurred between PTTCA and LPS, probably on a molecular level.

Figure 2e,f shows the SEM image and energy dispersive X-ray spectroscopy (EDS) mappings of the cross section of the pellet containing electrolyte and cathode layers. Compared to the LPS electrolyte layer with many voids, the PTTCA@CNT/SP/LPS cathode layer (with a thickness of ≈25 μm) was much more compact, demonstrating the intimate contact among active material, conductive carbon, and sulfide electrolyte. Besides the SEM image, the EDS mappings of P and S elements showed no observable crack at the interface of the two layers, indicating good mechanical contact between them, which is the prerequisite to achieve acceptable interface impedance and thereby reaction kinetics. In addition, for the cathode layer, it is also necessary to achieve sufficient electronic and ionic conduction by

optimizing the kind, proportion, and distribution of conductive carbon in the cathode composite. On one hand, sufficient contact between PTTCA and carbon was desired in addition to the well-formed carbon matrix. On the other hand, unnecessary contact between LPS and carbon should be avoided to suppress the side reactions[25] and alleviate the blocking to Li-ion diffusion. That was why we adopted an in situ polymerization method to introduce the majority (12.9 wt% of the whole cathode) of the conductive carbon, and then added the other minority (2.1 wt%). Direct-current polarization method was applied to study the influence of conductive carbon (SP or CNTs) on the electronic and ionic conductivities of the cathode pellet. The results are shown in Figure 2g and the original data are presented in Figures S4–S6 and Table S4, Supporting Information. It was found that the two cathode pellets exhibited almost the same ionic conductivity (around 4×10^{-7} S cm^{-1}), but very different electronic conductivities. The electronic conductivity of PTTCA@CNT/SP/LPS (4.4×10^{-5} S cm^{-1}) was two orders of magnitude higher than that of PTTCA@SP/SP/LPS (5.7×10^{-7} S cm^{-1}). Considering the same proportion and similar distribution, the remarkable difference should arise from the different specific surface areas (62 and 420 m^2 g^{-1} for SP and CNTs, respectively, according to the product information) and morphological features of SP and CNTs. Apparently, linear CNTs preferred to form a percolation network of electron compared to SP.

**ADVANCED
SCIENCE NEWS**

www.advancedsciencenews.com

**ADVANCED
ENERGY
MATERIALS**

www.advenergymat.de

Figure 3. Electrochemical performance of Li–PTTCA cells (unless otherwise specified, they were all-solid-state cells with a cathode composition of PTTCA/[CNT + SP]/LPS = 30:15:55, within the voltage range of 1.3–3.5 V vs Li$^+$/Li or equally 0.7–2.9 V vs In/InLi [$E_{In/InLi}$ = 0.6 V vs Li$^+$/Li], under a current rate of 50 mA g^{-1} at 25 °C): a) cycling performance and b,c) corresponding discharge–charge voltage profiles of PTTCA@SP and PTTCA@CNT in the all-solid-state cells, as well as PTTCA@CNT in the liquid cell (with a cathode composition of PTTCA/[CNT + SP]/PVDF = 60:30:10, and 1 M LiTFSI/DOL–DME electrolyte) for comparison; d) rate performance and e,f) corresponding discharge–charge voltage profiles of PTTCA@SP and PTTCA@CNT under different current rates (50, 100, 200, 300, 500 mA g^{-1}) at different temperatures (25 and 60 °C); g) CV curves of PTTCA@CNT at a scan rate of 0.05 mV s^{-1}; h) GITT curves of PTTCA@SP and PTTCA@CNT (2nd cycle), with a relaxation time of 1 h after each discharge or charge step of 5 min; i) Nyquist plots of the Li–PTTCA@CNT all-solid-state cell in pristine and discharged state at different cycle numbers (1st, 2nd, 5th, 10th, 20th, and 50th).

2.3. Electrochemical Performance of Poly(Trithiocyanuric Acid)-Based All-Solid-State Lithium Batteries

The electrochemical performance of PTTCA@SP and PTTCA@CNT was compared in the all-solid-state cells with a configuration shown in Figure 2a. In addition, the performance of PTTCA@CNT in the liquid electrolyte (1 M LiTFSI/DOL–DME) was also evaluated for revealing the impacts of solid and liquid electrolytes on organic cathode materials. The cutoff voltage range was set to be 0.7–2.9 V versus In/InLi for all-solid-state cells, or equally 1.3–3.5 V versus Li$^+$/Li for liquid cells, within which PTTCA could fully display its electroactivity while the decomposition side reactions (including reduction and oxidation) of LPS electrolyte were negligible. For conventional presentation and direct comparison, the voltages versus In/InLi for all-solid-state cells were converted to voltages versus

Li$^+$/Li ($E_{In/InLi}$ = 0.6 V vs Li$^+$/Li), but the former form was also retained by using a secondary vertical axis (**Figure 3**).

Figure 3a shows the cycling performance of different cells under a current rate of 50 mA g^{-1} at 25 °C, and their corresponding voltage curves are given in Figure 3b,c and Figure S8a, Supporting Information. In the liquid electrolyte, PTTCA@CNT delivered a high initial discharge capacity of 438 mAh g^{-1} (based on the weight of PTTCA, the same hereinafter), which was almost equal to its theoretical capacity (450 mAh g^{-1}). However, due to serious dissolution of discharged PTTCA (in Li$_3$TTCA form after a full discharge, Figure S7, Supporting Information), the capacity was retained only 40% after 100 cycles. In the solid electrolyte, PTTCA@SP showed an initial discharge capacity of only 219 mAh g^{-1}, which was retained 36% after 100 cycles. Surprisingly, PTTCA@CNT delivered discharge capacities of 468, 395, and 410 mAh g^{-1} at the 1st, 2nd, and 40th cycle, respectively.

**ADVANCED
SCIENCE NEWS**

www.advancedsciencenews.com
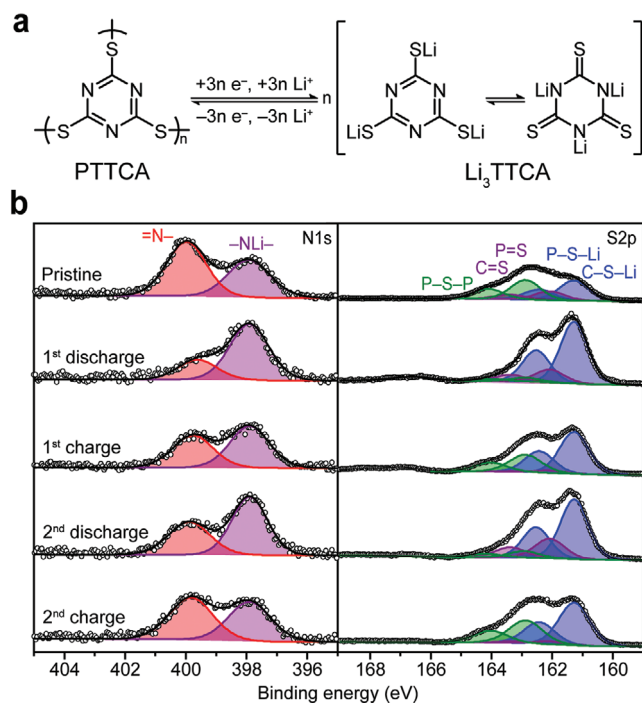
**ADVANCED
ENERGY
MATERIALS**

www.advenergymat.de

The latter value was regarded as the reversible capacity after activation and exclusion of side reactions of sulfide-electrolyte-based cells. Not only the reversible capacity set a new record for all-solid-state Li–organic batteries, the high utilization of 91% (relative to the theoretical capacity) was also rarely achieved, especially at room temperature. After 100 cycles of galvanostatic test spending about 2 months, the capacity retention still remained at 83%, which was an outstanding result for sulfide-electrolyte-based batteries. For the voltage profiles, PTTCA@CNT showed several voltage plateaus with an average discharge voltage of 2.4 V versus Li+/Li in the liquid electrolyte (Figure 3b), suggesting the high theoretical energy density (>1000 Wh kg^{-1}) and multistep reduction of PTTCA (the highest and major plateau at 2.6 V could be probably ascribed to the reaction from solid polymer to dissolved intermediate oligomers). In the solid electrolyte, it displayed only a sloping discharge curve with an average voltage of 1.8 V, suggesting a solid–solid reaction similar to those of other organic[5b] and sulfur[26] cathodes in sulfide electrolytes. In spite of the remarkable discharge voltage polarization (0.6 V) compared to the liquid cell and voltage gap (0.9 V) between discharge and charge processes (these will be discussed later), the high repeatability of voltage profiles indicated the high redox reversibility of PTTCA in the all-solid-state cells. For the Coulombic efficiency of PTTCA@CNT (Figure 3a), it stabilized at only 96% in the liquid electrolyte because of the shuttle effect (in charge process, dissolved PTTCA oligomers diffused to the Li anode and was reduced to lower-molecular-weight species, which moved back to the cathode to be oxidized again and led to extra charge capacity), which was completely eliminated in the solid electrolyte as suggested by the average value of 100.3% after the initial cycle.

Figure 3d compares the rate performance of PTTCA@SP at 25 °C and PTTCA@CNT at 25 and 60 °C. The corresponding voltage curves under different current rates are presented in Figure 3e,f and Figure S8b, Supporting Information. Reasonably, PTTCA@SP showed a poor rate capability that no capacity was released when the current rate exceeded 100 mA g^{-1}. PTTCA@CNT showed a much better rate performance with capacity retentions (relative to the reversible capacity under 50 mA g^{-1}) of 81%, 61%, 49%, and 33% at 100, 200, 300, and 500 mA g^{-1}, respectively. At an elevated temperature of 60 °C, PTTCA@CNT exhibited slightly improved capacity retentions, but considerably increased reversible capacity with an increment of ≈110 mAh g^{-1} under each current rate. It is worth noting that its capacity reached 510 mAh g^{-1} at 50 mA g^{-1}, obviously exceeding the theoretical capacity of PTTCA (450 mAh g^{-1}). Considering that LPS electrolyte might also contribute some reversible capacity due to its electroactivity,[27] we replaced PTTCA by poly(vinylidene fluoride) (PVDF) as an inactive polymer (Figure S9a,b, Supporting Information) to investigate the electrochemical performance of merely LPS with similar distribution of CNTs. The result (Figure S9c,d, Supporting Information) showed reversible capacities of 7 and 80 mAh g^{-1} (based on the weight of PVDF) at 25 and 60 °C, respectively, which could be regarded as the capacity contribution of LPS to PTTCA@CNT/SP/LPS electrode. It indicated that the capacity increment was majorly from the facilitated side reactions of LPS, and minorly from the promoted reaction kinetics of PTTCA (with a utilization up to 96%) at higher

temperature. In addition, the voltage polarization was significantly alleviated that its discharge voltage increased by about 0.2 V at 60 °C under each current rate.

Besides the galvanostatic discharge–charge tests, other electrochemical techniques were also applied to analyze the electrochemical behaviors of PTTCA in the all-solid-state cells. Figure 3g shows the cyclic voltammetry (CV) curves of PTTCA@CNT at a scan rate of 0.05 mV s^{-1}. Similar to the discharge–charge curves (Figure 3c), except the larger voltage polarization shown in the first reduction process, the subsequent processes displayed highly consistent curves with a pair of redox peaks at 1.9/2.9 V. Obviously, relatively stable micro architectures involving the interfaces between PTTCA and LPS, were formed after the necessary adjustment during the first discharge, facilitating the redox reaction kinetics in the following cycles. Figure 3h shows the galvanostatic intermittent titration technique (GITT) curves of PTTCA@SP and PTTCA@CNT, and their corresponding polarization voltage plots are presented in Figure S10, Supporting Information. Generally, the average discharge/charge polarization voltages were 0.7/0.4 V for PTTCA@SP and 0.3/0.3 V for PTTCA@CNT, respectively. It verified the faster redox reaction kinetics of PTTCA@CNT benefiting from the much higher electronic conductivity (Figure 2g). Moreover, the quasi-open-circuit voltage plots were not coincided between discharge and charge process (with average voltage gaps of about 0.3 and 0.4 V for PTTCA@SP and PTTCA@CNT, respectively), suggesting that the reaction routes were not completely reversible. Figure 3i shows the electrochemical impedance spectroscopy (EIS) data of Li–PTTCA@CNT all-solid-state cell in pristine and discharged state at different cycle numbers, and the corresponding equivalent circuit and fitted parameters are summarized in Table S5, Supporting Information. The solid electrolyte resistance (R_{SE}) kept at a relatively low value of 24.0–28.8 Ω during the whole test, indicating that Li+ diffusion in bulk solid electrolyte particles was not a major factor influencing the reaction kinetics and cycling stability. The high-frequency resistance (R_{HF}) attributed to the interfacial charge transfer between PTTCA and LPS was also relatively stable (177, 135, 153, and 197 Ω at the 1st, 2nd, 10th, and 50th cycle, respectively), suggesting that the contact degradation caused by volume expansion/shrinkage of PTTCA was not so serious,[28] probably because of the soft interface and the coordination interaction between the active material and solid electrolyte (Figure 2a). On the contrast, the middle-frequency and low-frequency resistances (R_{MF} and R_{LF}) increased more significantly (from 180/139 Ω at 1st cycle to 355/248 Ω at 50th cycle for R_{MF}/R_{LF}), which responded to the decomposition product accumulation of LPS[29] and mechanical failure of InLi anode,[28] respectively. In Figure 3a, it was found that the average Coulombic efficiency exceeded 100% even after excluding the initial one or ten cycles (100.3% or 100.2%, respectively), which was a clue of the minor but persistent reduction decomposition of LPS electrolyte, in consistence with the above analysis of R_{MF}. It was probably the main origin of capacity decay of the all-solid-state cell (in Figure 3a, the capacity decay was offset by the activation process in the former 50 cycles, and then became more obvious in the latter 50 cycles). Therefore, to improve the long-term cycling stability, we should further reduce the side reactions of the solid electrolyte, by suppressing the contact

**ADVANCED
SCIENCE NEWS**

www.advancedsciencenews.com

**ADVANCED
ENERGY
MATERIALS**

www.advenergymat.de

Figure 4. a) Electrochemical redox reaction of PTTCA. b) XPS spectra (N1s and S2p) of PTTCA@CNT/SP/LPS cathodes in different states (pristine, after 1st discharge and charge, and after 2nd discharge and charge).
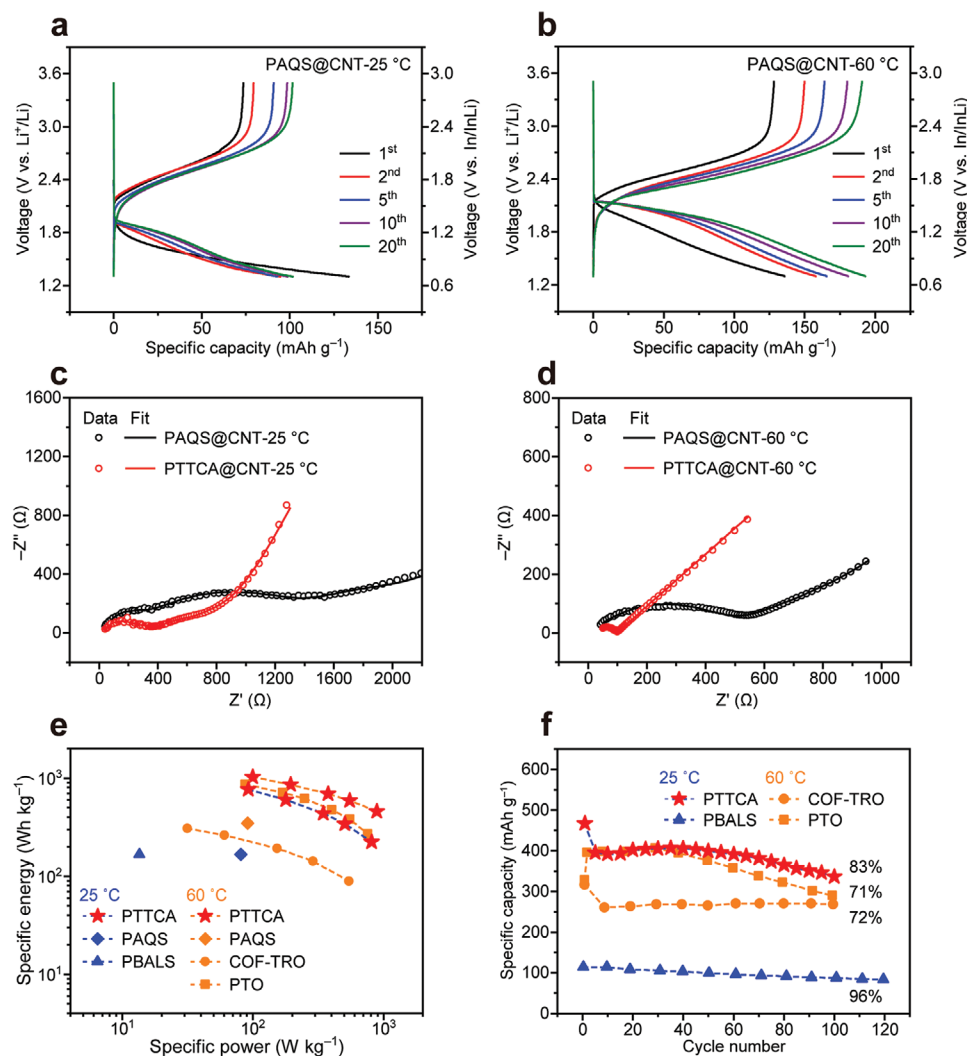
between LPS and conductive carbon, or choosing a sulfide electrolyte with higher electrochemical stability.

2.4. Redox Reaction and Electrode Evolution Mechanisms

To study the redox reaction (proposed in **Figure 4**a) and electrode evolution mechanisms of PTTCA@CNT/SP/LPS cathode, we tested the XPS spectra of the electrodes in different states including pristine, discharged, and charged at the 1st and 2nd cycle (Figure 4b). After the 1st discharge, the relative intensity of −NLi− increased while that of =N− decreased, in consistence with the formation of thione-like Li_3TTCA. Meanwhile, in the S2p spectra, the proportions of peaks at 161.3 and 162.1 eV (ascribed to the $2p_{3/2}$ peaks of P−S···Li/C−S···Li and P=S/C=S forms, respectively) both increased while the peak at 162.9 eV (ascribed to the $2p_{3/2}$ peak of P−S−P) decreased, agreeing with the formation of thiol-like Li_3TTCA and the reduction of interphase constituents between PTTCA and LPS (from $P_2S_7^{4-}$ to PS_4^{3-}).[8b] The N1s and S2p spectra varied in an inverse way during the subsequent charge process, however, resulting in less =N− but more P−S···Li/C−S···Li structures compared to the pristine state. It implied that partial Li_3TTCA produced in the 1st discharge was unable to revert to PTTCA, possibly due to its poor electronic conductivity[30] or strong coordination interaction between Li_3TTCA and LPS. It was also consistent to the higher Coulombic efficiency (120.5%) of PTTCA@CNT in the 1st cycle (Figure 3a). In the 2nd cycle, the XPS peak variations almost repeated those of the 1st cycle, verifying the high reversibility of electrode evolution once a relatively stable interface was built between active material and sulfide electrolyte.

2.5. Comparison between Organodisulfide and Carbonyl Cathodes in All-Solid-State Lithium Batteries

As discussed in the introduction part, we speculate that organodisulfides are more compatible with sulfide electrolyte than carbonyl compounds based on the HSAB theory. To confirm this speculation, we have also tested a typical carbonyl polymer, namely PAQS, in the same way as for PTTCA. PAQS@CNT composite was also synthesized by an in situ polymerization method[31] (Figure S11a, Supporting Information), and the chemical structure was confirmed by FT-IR spectra (Figure S11b and Table S6, Supporting Information). TG analysis (Figure S11c, Supporting Information) revealed a PAQS content of 72% in the composite, while SEM and TEM images (Figure S12, Supporting Information) showed a morphology of well-distributed PAQS and CNTs, both of which were similar to PTTCA@CNT composite. The PAQS@CNT sample was first tested in the liquid cell and demonstrated an ideal reversible capacity (close to the theoretical capacity of 225 mAh g^{-1}) and cycling stability, verifying its successful synthesis and good architecture. However, in the all-solid-state cell with similar cathode composition and fabrication as for PTTCA@CNT, it could release a reversible capacity of only 101 mAh g^{-1} at 25 °C after 20 cycles of activation (**Figure 5**a). Compared to PTTCA@CNT, the utilization of active material (45%) was much lower and the activation process was much longer, indicating much poorer redox kinetics of PAQS in ASSLBs. At a higher temperature of 60 °C, the reversible capacity was elevated to 193 mAh g^{-1} (Figure 5b); however, it corresponds to a low utilization of only 50% after subtraction of the capacity contribution (80 mAh g^{-1}) of LPS at 60 °C (Figure S9d, Supporting Information). Similar to PTTCA@CNT, the high initial Coulombic efficiency (181.4%) of PAQS@CNT implied the strong and irreversible interaction between PAQS and LPS, which was greatly diminished at 60 °C. For a clearer understanding of the reaction kinetics, we compared the EIS data (after the first discharge) of PAQS and PTTCA at the two different temperatures (Figure 5c,d, detailed equivalent circuits and fitted parameters are presented in Tables S7 and S8, Supporting Information). At 25 °C, the R_{MF} of PAQS@CNT (1110 Ω) attributed to the decomposition product accumulation of LPS, was nearly six times as that of PTTCA@CNT (180 Ω). At 60 °C, the 3(RQ) equivalent circuit model (Table S7, Supporting Information) could be simplified into the RQ model (Table S8, Supporting Information) owing to the overlapping time constants of the electrochemical processes at high temperature.[32] Therefore, the interface resistance, R_{int}, was defined as the sum of R_{HF}, R_{MF}, and R_{LF}. It was found that the R_{int} of PAQS@CNT decreased from 1487 Ω at 25 °C to 453 Ω at 60 °C, however, still about five times as that of PTTCA@CNT (88.3 Ω). These results indicated that the interface side reactions between PAQS and LPS were much more serious than those between PTTCA and LPS. In another word, organodisulfide cathode materials have much better compatibility with sulfide electrolyte than carbonyl materials, possibly because of the catalytic effects of them to each other's redox reaction in ASSLBs. Besides PAQS, the electrochemical performance of PTTCA was also compared with that of other reported organic cathode materials applied in ASSLBs using sulfide electrolytes, including carbonyl-type COF-TRO[7] and PTO,[8a] and azo-type

**ADVANCED
SCIENCE NEWS**

www.advancedsciencenews.com

**ADVANCED
ENERGY
MATERIALS**

www.advenergymat.de

Figure 5. a,b) Discharge–charge voltage profiles of PAQS@CNT cathode in ASSLBs (PAQS/[CNT + SP]/LPS = 30:15:55, 0.7–2.9 V vs In/InLi, 50 mA g^{-1}) at 25 and 60 °C, respectively. c,d) Nyquist plots of Li–PAQS@CNT and Li–PTTCA@CNT cells after the 1st discharge at 25 and 60 °C, respectively. e) Ragone plot and f) cycling performance comparison of PTTCA with PAQS and other previously reported organic cathode materials for sulfide-electrolyte-based ASSLBs (all data were based on the weight of cathode active material, and the capacity retentions were relative to the reversible capacity rather than the 1st discharge capacity).

PBALS[9] (Figure 5e,f, detailed information is listed in Table S9, Supporting Information). Obviously, the comprehensive electrochemical performance (including reversible capacity, energy density, cycling stability, and rate capability) of PTTCA at 25 °C, was approaching or even superior to that of PTO at 60 °C, which represented the state-of-the-art technology of all-solid-state Li–organic batteries. In addition to the exciting battery performance at room temperature, the much easier synthesis and lower cost make organodisulfide one of the most promising types of organic cathode materials for ASSLBs. Of course, there is still a long way to go for practical application. For example, the cathode composition and architecture need further optimization to simultaneously realize higher mass ratio and loading of active material, as well as lower voltage polarization in discharge–charge process.

3. Conclusion

In this work, PTTCA was investigated as the first organodisulfide cathode material for ASSLBs and achieved outstanding electrochemical performance among all organic cathode materials. First, CNTs were introduced by an in situ polymerization method to enhance the electronic conductivity of the cathode composite. Second, the Li$^+$···N coordination interaction between PTTCA cathode and LPS electrolyte facilitated their intimate contact. Third, PTTCA showed much better interface compatibility with LPS than carbonyl-type PAQS, which could be explained by the HSAB theory and possible catalytic effects of them to each other. Benefiting from the above advantages, PTTCA demonstrated the most remarkable electrochemical performance for all-solid-state Li–organic batteries,

ADVANCED
SCIENCE NEWS

www.advancedsciencenews.com

ADVANCED
ENERGY
MATERIALS

www.advenergymat.de

especially at room temperature. The reversible capacity reached 410 mAh g^{-1} under a current rate of 50 mA g^{-1}, corresponding to a high active material utilization of 91% and a high energy density of 767 Wh kg^{-1}. After 100 cycles of discharge–charge test (over 2 months), the capacity retention still remained 83% (relative to 410 mAh g^{-1}), verifying that the dissolution problem of PTTCA (in discharged forms) no longer existed in ASSLBs. These results reveal that the combination of organodisulfide cathodes and sulfide electrolytes provides both of them new developing opportunities, toward the practical application of all-solid-state Li–organic batteries.

4. Experimental Section

Material Preparations: All the raw materials and reagents were commercially purchased and used as received without further purification. PTTCA was synthesized by a modified method according to the previous reports.[14a,15] First, TTCA (1.00 g, 5.64 mmol, Adamas) and LiOH (0.406 g, 16.9 mmol, Adamas) were mixed in 100 mL deionized water to get a clear solution of trithiocyanuric acid trilithium salt (Li$_3$TTCA). After adding 10 mL saturated aqueous solution of KI (16.1 g, Chemxyz) containing iodine (I$_2$, 3.22 g, 12.7 mmol, Energy Chemical) as oxidizer, the solution was intensely stirred overnight at 0 °C. The precipitate was collected by filtration, washed with deionized water, ethanol, and acetone subsequently. The product was dried at 80 °C under vacuum for 12 h, affording a pale-yellow powder with a yield of 80%.

In order to improve the electronic conductivity, PTTCA@SP and PTTCA@CNT composites were synthesized by an in situ polymerization method. A quantity (0.379 g) of SP or CNTs (multiwalled, 5–20 nm in diameter, 10–20 μm in length, Timesnano) was added into the same Li$_3$TTCA solution as above. To facilitate the dispersion of CNTs in aqueous solution, some dispersant (TNWDIS, 0.190 g, Timesnano) was also added into the solution. The mixture was sonicated by a probe sonicator (JY92-IIN, Scientz, China) for 2 h at 0 °C, followed by the same processes as above from adding I$_2$–KI solution to vacuum drying. Finally, a black powder containing ≈70 wt% PTTCA (determined by either TG or EA) were obtained with a yield of 90% (based on the amount of TTCA) for both two composites.

For comparison, PAQS@CNT composite was also synthesized by an in situ polymerization method according to the previous reports.[31,33] First, 1,5-dichloranthraquinone (DCAQ, 1.00 g, 3.60 mmol, Adamas) and CNTs (0.286 g) were added into 50 mL *N*-methylpyrrolidone (NMP) and the mixture was sonicated for 1 h. After adding anhydrous Li$_2$S (0.166 g, 3.60 mmol, Strem) into the mixture, the reaction proceeded under refluxing at 200 °C and stirring overnight. The precipitate was collected by centrifugation after cooling to room temperature, washed with NMP, deionized water, and acetone subsequently. The product was dried at 150 °C under vacuum for 12 h, affording a black powder containing ≈72 wt% PAQS (determined by TG analysis) with a yield of 98% (based on the amount of DCAQ).

To evaluate the capacity contribution of CNTs, PVDF@CNT composite was prepared by a solution blending method. Typically, PVDF (0.300 g, M_w = 1.0 × 10^6 g mol^{-1}, Arkema) and CNTs (0.100 g) were mixed in 5 mL NMP, and the mixture was sonicated for 6 h. After evaporating the NMP solvent at 150 °C, a black powder was obtained as the composite.

Material Characterizations: FT-IR spectra were recorded using KBr pellets on an ALPHA II spectrometer (Bruker, Germany) in the wavenumber range of 400–4000 cm^{-1}. Raman spectra were recorded on a DXR2 Raman microscope (Thermo Scientific, USA) using a 532 nm excitation laser and a 0.5 mW laser power to avoid heating and destruction. Powder XRD patterns were collected by a MiniFlex 600 X-ray diffractometer (Rigaku, Japan) with Cu Kα1 radiation (λ = 1.5406 Å), in the 2θ range of 5–60° at a scan rate of 10° min^{-1}. The XPS analysis was carried out on a K-Alpha+ spectrometer (Thermo Scientific, USA)

using monochromated Al Kα radiation ($h\nu$ = 1486.6 eV). TG analysis was conducted on a TG 209 F1 Libra thermal analyzer (NETZSCH, Germany) under nitrogen atmosphere, in the temperature range of 25–800 °C at a heating rate of 10 °C min^{-1}. EA (CHNS mode) was conducted on a Vario El Cube element analyzer (Elemantar, Germany). SEM observations and EDS mapping were performed on a MERLIN Compact microscopy (Zeiss, Germany). TEM observations were performed on a JEM-2100 Plus microscopy (Joel, Japan).

Liquid Cell Fabrications: PTTCA@CNT or PAQS@CNT composite was mixed with SP and PVDF in NMP solvent to form a homogeneous slurry, with the composition of 60 wt% active material (PTTCA or PAQS), 30 wt% conductive carbon (CNTs and SP), and 10 wt% binder (PVDF). The electrode film was prepared by casting the slurry onto a carbon-coated aluminum foil using a doctor blade and drying at 80 °C under vacuum overnight. The electrode film was punched into small discs (ϕ = 12 mm) with typical active material loading of 1.5 mg cm^{-2}. CR2025-type coin cells were assembled by using the disc as cathode, a piece of Li foil (ϕ = 14.0 mm, δ = 0.40 mm) as anode, a Celgard 2500 membrane as separator, and 1 M LiTFSI/DOL–DME (lithium bis(trifluoromethanesulfonyl)imide dissolved in the mixture of 1,3-dioxolane and 1,2-dimethoxyethane, with the volume ratio of 1:1) as electrolyte.

All-Solid-State Cell Fabrications: For all-solid-state cells, the cathode composites (PTTCA@SP/SP/LPS, PTTCA@CNT/SP/LPS, PVDF@CNT/SP/LPS, and PAQS@CNT/SP/LPS) were prepared with optimized composition of 30 wt% active material (PTTCA, PAQS, or PVDF as a reference), 15 wt% conductive carbon (CNTs and SP), and 55 wt% sulfide electrolyte (LPS, MTI). Typically, 170 mg PTTCA@CNT, 8.6 mg SP, and 220 mg LPS were well mixed by a Pulverisette 7 ball mill (Fritsch, Germany) using a 50 mL ZrO$_2$ jar with 24 g ZrO$_2$ balls (ϕ = 5 mm), at 600 rpm for 36 h. To assemble the cell, 120 mg LPS powder was filled into a polyetheretherketone die with an inner diameter of 12 mm, and pressed under a pressure of 180 MPa to form a pellet. Then, 4.5 mg of the cathode composite (corresponding to an active material loading of 1.2 mg cm^{-2}) was uniformly distributed on one side of the LPS pellet, and pressed under a pressure of 380 Mpa for 5 min. Finally, a piece of In foil (ϕ = 11 mm, δ = 100 μm) and a piece of Li foil (ϕ = 10 mm, δ = 60 μm) were put on the other side of the LPS pellet in sequence, and all layers were pressed together under a pressure of 100 Mpa for 1 min. The as-prepared Swagelok cell with two stainless steel cylinders as current collectors was directly tested in an external clamp with an initial pressure of 0.5 Mpa (adjusted by a torque wrench). The pellet (δ = 1.0 mm) containing cathode and electrolyte layers was also taken out for characterizations. Symmetric cells with configurations showed in Figures S4a, S5a, and S6, Supporting Information, were similarly fabricated for electronic and ionic conductivity measurements. All the above processes were conducted in an argon-filled glove box with moisture and oxygen contents <1 ppm.

Electrochemical Tests: The galvanostatic discharge–charge and GITT tests of the above liquid and all-solid-state cells were carried out on a CT2001A battery test system (LANHE, China), within the voltage range of 1.3–3.5 V versus Li$^+$/Li or equally 0.7–2.9 V versus In/InLi ($E_{In/InLi}$ = 0.6 V vs Li$^+$/Li). The GITT tests were conducted at a current rate of 50 mA g^{-1}, with a relaxation time of 1 h after each discharge or charge step of 5 min. The CV, direct-current polarization, and EIS tests of the all-solid-state cells were performed on a PRATAT MC electrochemical station (Princeton Applied Research, USA). The CV tests were conducted within the voltage range of 0.7–2.9 V versus In/InLi at a scan rate 0.05 mV s^{-1}. The direct-current polarization measurements of symmetric cells were conducted by reference to the previous report.[34] For electronic conductivity (σ_{el}), constant potentials of 5, −10, 20, and −30 mV were applied for 6 h for each potential. For ionic conductivity (σ_{ion}), constant potentials of 60 and −40 mV were applied for 12 h for each potential. The EIS tests were conducted for the symmetric cells containing LPS pellets to evaluate the ionic conductivity, and common all-solid-state cells in discharged state to analyze the reaction kinetics, with the frequency range of 7 × 10^6–1 × 10^{-2} Hz and a voltage amplitude of 20 mV. All the conductivities (σ, S cm^{-1}) were calculated by the following equation,

ADVANCED
SCIENCE NEWS

www.advancedsciencenews.com

ADVANCED
ENERGY
MATERIALS

www.advenergymat.de

$$\sigma = \frac{\delta}{R \times A} = \frac{\delta}{R \times \left(\frac{\phi}{2}\right)^2 \times 3.14} \tag{1}$$

where R (Ω) referred to the resistance of the sample pellet measured by electrochemical tests, and A (cm^2), ϕ (cm), and δ (cm) referred to the area, diameter, and thickness of the pellet, respectively. All the above electrochemical tests were operated at room temperature (25 °C), but for the galvanostatic discharge–charge tests of all-solid-state cells, 60 °C was also applied for comparison.

Ex Situ Electrode Characterizations: PTTCA@CNT/SP/LPS electrodes in different states (pristine, discharged, and charged of the 1st and 2nd cycle) were harvested from the disassembled all-solid-state cells after specified discharge–charge processes at 50 mA g^{-1}. XPS analysis of the cathode surface was carried out using the same spectrometer and conditions as mentioned above. The electrodes were well protected in glove box or tightly sealed aluminum-plastic bags before characterization.

Conflict of Interest

The authors declare no conflict of interest.

Data Availability Statement

Research data are not shared.

[1] B. Esser, F. Dolhem, M. Becuwe, P. Poizot, A. Vlad, D. Brandell, *J. Power Sources* **2021**, *482*, 228814.
[2] K. Zhang, C. Guo, Q. Zhao, Z. Niu, J. Chen, *Adv. Sci.* **2015**, *2*, 1500018.
[3] Z. Song, Y. Qian, M. L. Gordin, D. Tang, T. Xu, M. Otani, H. Zhan, H. Zhou, D. Wang, *Angew. Chem., Int. Ed.* **2015**, *54*, 13947.
[4] T. Cai, Y. Han, Q. Lan, F. Wang, J. Chu, H. Zhan, Z. Song, *Energy Storage Mater.* **2020**, *31*, 318.
[5] a) J. Heiska, M. Nisula, M. Karppinen, *J. Mater. Chem. A* **2019**, *7*, 18735; b) L. Zhao, A. E. Lakraychi, Z. Chen, Y. Liang, Y. Yao, *ACS Energy Lett.* **2021**, *6*, 3287.
[6] R. Chen, Q. Li, X. Yu, L. Chen, H. Li, *Chem. Rev.* **2020**, *120*, 6820.
[7] X. Yang, Y. Hu, N. Dunlap, X. Wang, S. Huang, Z. Su, S. Sharma, Y. Jin, F. Huang, X. Wang, S.-h. Lee, W. Zhang, *Angew. Chem., Int. Ed.* **2020**, *59*, 20385.
[8] a) F. Hao, Y. Liang, Y. Zhang, Z. Chen, J. Zhang, Q. Ai, H. Guo, Z. Fan, J. Lou, Y. Yao, *ACS Energy Lett.* **2020**, *6*, 201; b) J. Zhang, Z. Chen, Q. Ai, T. Terlier, F. Hao, Y. Liang, H. Guo, J. Lou, Y. Yao, *Joule* **2021**, *5*, 1845.
[9] C. Luo, X. Ji, J. Chen, K. J. Gaskell, X. He, Y. Liang, J. Jiang, C. Wang, *Angew. Chem., Int. Ed.* **2018**, *130*, 8703.
[10] G. Sahu, Z. Lin, J. Li, Z. Liu, N. Dudney, C. Liang, *Energy Environ. Sci.* **2014**, *7*, 1053.
[11] H. Muramatsu, A. Hayashi, T. Ohtomo, S. Hama, M. Tatsumisago, *Solid State Ionics* **2011**, *182*, 116.
[12] a) X. Chi, Y. Liang, F. Hao, Y. Zhang, J. Whiteley, H. Dong, P. Hu, S. Lee, Y. Yao, *Angew. Chem., Int. Ed.* **2018**, *57*, 2630; b) F. Hao, X. Chi, Y. Liang, Y. Zhang, R. Xu, H. Guo, T. Terlier, H. Dong, K. Zhao, J. Lou, Y. Yao, *Joule* **2019**, *3*, 1349.
[13] D. Wang, W. Guo, Y. Fu, *Acc. Chem. Res.* **2019**, *52*, 2290.
[14] a) M. Liu, S. J. Visco, L. C. D. Jonghe, *J. Electrochem. Soc.* **1991**, *138*, 1891; b) X. Tu, Z. Wu, X. Geng, L. Qu, H. Sun, C. Lai, D. Li, S. Zhang, *J. Mater. Chem. A* **2021**, *9*, 18306.
[15] X. Li, C. Bian, X. Meng, F. Xiao, *J. Mater. Chem. A* **2016**, *4*, 5999.
[16] M. Kucharski, E. Chmiel-Szukiewicz, *J. Appl. Polym. Sci.* **2000**, *76*, 439.
[17] J. Xu, L. Luo, G. Xiao, Z. Zhang, H. Lin, X. Wang, J. Long, *ACS Catal.* **2014**, *4*, 3302.
[18] H. E. Van Wart, A. Lewis, H. A. Scheraga, F. D. Saeva, *Proc. Natl. Acad. Sci. U. S. A.* **1973**, *70*, 2619.
[19] A. L. Santhosha, J. R. Buchheim, P. Adelhelm, *Batteries Supercaps* **2019**, *2*, 524.
[20] W. Fu, Z. Huang, *ACS Sustainable Chem. Eng.* **2018**, *6*, 14785.
[21] N. Alam, M. Sreeramareddygari, M. Somasundrum, K. Jayaramulu, W. Surareungchai, *ChemistrySelect* **2021**, *6*, 5140.
[22] R. Koerver, F. Walther, I. Ayguen, J. Sann, C. Dietrich, W. G. Zeier, J. Janek, *J. Mater. Chem. A* **2017**, *5*, 22750.
[23] R. S. Vishwanath, S. Kandaiah, *J. Mater. Chem. A* **2017**, *5*, 2052.
[24] K. Lee, S. Kim, J. Park, S. H. Park, A. Coskun, D. S. Jung, W. Cho, J. W. Choi, *J. Electrochem. Soc.* **2017**, *164*, A2075.
[25] T. Hakari, Y. Sato, S. Yoshimi, A. Hayashi, M. Tatsumisago, *J. Electrochem. Soc.* **2017**, *164*, A2804.
[26] W.-P. Wang, J. Zhang, J. Chou, Y.-X. Yin, Y. You, S. Xin, Y.-G. Guo, *Adv. Energy Mater.* **2021**, *11*, 2000791.
[27] G. F. Dewald, S. Ohno, M. A. Kraft, R. Koerver, P. Till, N. M. Vargas-Barbosa, J. Janek, W. G. Zeier, *Chem. Mater.* **2019**, *31*, 8328.
[28] W. Zhang, D. Schroeder, T. Arlt, I. Manke, R. Koerver, R. Pinedo, D. A. Weber, J. Sann, W. G. Zeier, J. Janek, *J. Mater. Chem. A* **2017**, *5*, 9929.
[29] W. Zhang, T. Leichtweiss, S. P. Culver, R. Koerver, D. Das, D. A. Weber, W. G. Zeier, J. Janek, *ACS Appl. Mater. Interfaces* **2017**, *9*, 35888.
[30] L.-P. Hou, H. Yuan, C.-Z. Zhao, L. Xu, G.-L. Zhu, H.-X. Nan, X.-B. Cheng, Q.-B. Liu, C.-X. He, J.-Q. Huang, Q. Zhang, *Energy Storage Mater.* **2019**, *25*, 436.
[31] Z. Song, T. Xu, M. L. Gordin, Y.-B. Jiang, I.-T. Bae, Q. Xiao, H. Zhan, J. Liu, D. Wang, *Nano Lett.* **2012**, *12*, 2205.
[32] P. Vadhva, J. Hu, M. J. Johnson, R. Stocker, M. Braglia, D. J. L. Brett, A. J. E. Rettie, *ChemElectroChem* **2021**, *8*, 1930.
[33] Z. Song, H. Zhan, Y. Zhou, *Chem. Commun.* **2009**, *4*, 448.
[34] G. F. Dewald, S. Ohno, J. G. C. Hering, J. Janek, W. G. Zeier, *Batteries Supercaps* **2021**, *4*, 183.